

Gamma-Ray Imaging Using a CdZnTe Pixel Array and a High-Resolution, Parallel-Hole Collimator.

GA Kastis^{1,2}, HB Barber^{1,2}, HH Barrett^{1,2}, SJ Balzer^{1,2}, D Lu^{1,2}, DG Marks^{1,2},
G Stevenson¹, JM Woolfenden¹, M Appleby³, J Tueller⁴.

¹ Department of Radiology, Division of Nuclear Medicine, University of Arizona, Tucson, AZ 85724

² Optical Sciences Center, University of Arizona, Tucson, AZ 85721

³ Tecomet, Woburn, MA 01801

⁴ NASA Goddard Spaceflight Center, Greenbelt, MD 20771

Abstract

The poor performance of current parallel-hole collimators is an impediment to planar high-resolution gamma-ray imaging, even when high-resolution semiconductor detector arrays are available. High-resolution parallel-hole collimators are possible but have not been fabricated because current collimator construction techniques severely limit achievable bore size and septal thickness. We describe development and testing of a high-resolution collimator with 4096 260- μm square bores and 380 μm pitch, matched to our existing 2.5 cm \times 2.5 cm hybrid 64 \times 64 CdZnTe arrays with multiplexer readout. The collimator is a laminar composite of about 100 layers of W sheets produced by photolithography and has efficiency of 5×10^{-5} . We have demonstrated sub-millimeter spatial resolution at 140 keV in both phantom and animal imaging using this system. Images resolved individual vertebrae in the spine of a mouse and lymphatic channels and nodes in a rat. The collimator and semiconductor array could form a compact module for use in a wide variety of gamma-ray imaging systems.

I. INTRODUCTION

There is a need for high-resolution gamma-ray imaging systems for small animals for use in molecular medicine. The principal tracer techniques used in animals are tissue counting in vitro and autoradiography. Both are labor intensive and time consuming, and the requirement to sacrifice the animal precludes longitudinal studies in a single animal. Nuclear medicine imaging techniques are an attractive alternative but will require a major improvement in spatial resolution to be useful in this application. Gamma-ray imaging systems with about 2-mm spatial resolution have recently been reported [1], [2]. The use of semiconductor detector arrays is a promising route to making ultra-high-resolution detectors to replace scintillators in gamma cameras [3]-[6]. Semiconductor detectors such as CdZnTe are attractive because they can be partitioned into high-resolution detector arrays using photolithography techniques. We have developed practical techniques for reading out such large pixel arrays using integrated circuits bonded directly to the pixel arrays [7]. High-resolution imaging will also require improvement of the imaging aperture, in this case a multi-bore collimator. Until

recently, the technology for making efficient collimators with sufficiently small bore-size was not available. Here we describe the development of a semiconductor-detector array and compatible multi-bore collimator and demonstrate their use in high-resolution, planar gamma-ray imaging of small animals.

II. IMAGING SYSTEM

A. 64 \times 64 CdZnTe Detector Module

Our group has been active in developing high-resolution CdZnTe semiconductor arrays for use in nuclear medicine [8]-[11]. A 64 \times 64 Cd_{0.9}Zn_{0.1}Te detector module is shown in Figure 1. The detector array is a 2.5 cm \times 2.5 cm slab of CdZnTe with a thickness of 1.5 mm and a 64 \times 64 square array of gold electrodes on one side. The other side has a continuous gold electrode held at a constant bias of -140 V. The detector array has a pixel pitch of 380 μm , with a pixel size of 330 μm and an interpixel gap of 50 μm . The interpixel gap was chosen to increase the resistive isolation of the pixels. Each pixel of the detector array is electrically connected to a gated integrator in the readout circuit by an indium-bump bond. Individual pixels are multiplexed to a single output line and are read out in a raster scan. The integration time was 1 msec. The approach detects individual gamma interactions with excellent energy resolution and a spatial resolution of 380 μm or better. The current setup consists of a 2 \times 2 array of hybrid detectors housed in an aluminum box with lead shielding surrounding the box. Each detector is cooled to -15°C via thermoelectric coolers mounted under the arrays. Dry nitrogen is circulated through the box to eliminate moisture due to condensation. Only a single array was used for imaging in this work. The development and testing of this device have been reported elsewhere [9]-[11].

B. High-Resolution Collimator

Until recently, an important limitation in making high-resolution semiconductor imaging systems was the fabrication of a collimator with bores and septa fine enough to utilize the intrinsic spatial resolution properties of the arrays. The practice of stacking photochemically etched tungsten foils has

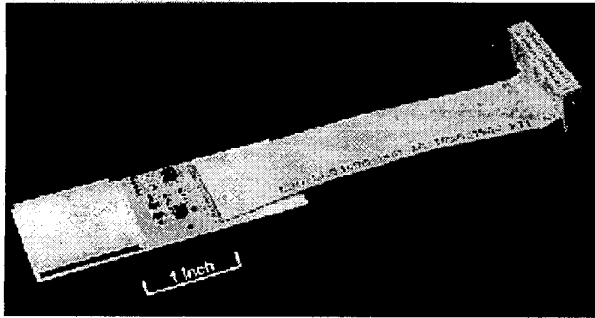


Figure 1: Photograph of the daughter board with the CdZnTe array and gated integrator mounted at the end [10].

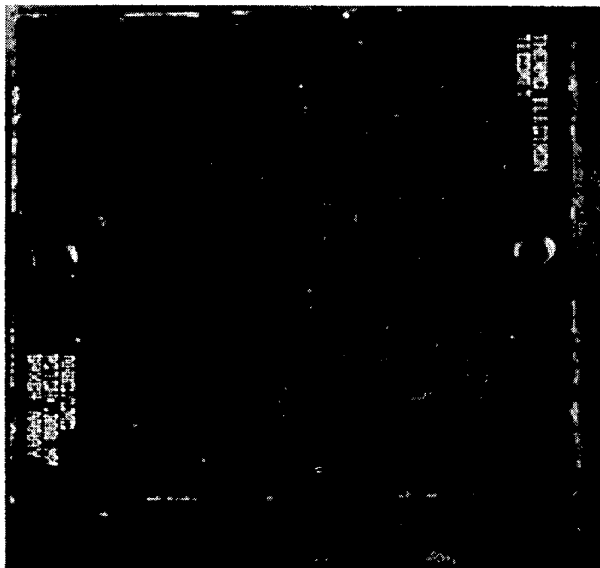


Figure 2: Photograph of the Tecomet collimator.

been used for fabricating specialized collimators [12]. The limitations of this practice have included the requirement for precise layer-to-layer stacking registration, bonding methods that provide clear cell passage, straight and uniform septa and feature sizes that are fine enough to meet resolution needs. In our case 75- μm tungsten foils were etched to form the collimator pattern. This foil thickness was used to provide straight and uniform etched contours through the collimator cells and septa. The foils were then assembled in precise alignment and epoxy bonded to form the integral array. A bonding process was used which leaves the collimator cells unobstructed in the final assembly. By combining a precise lamination technique with photochemical etching of the tungsten layers, distortion between layers is negligible. The positional accuracy from cell to cell on the final assembled collimator was $< 2 \mu\text{m}$.

We designed a tungsten parallel-hole collimator that exactly matches the pitch of the detector array. The collimator

is shown in Figure 2 and was fabricated by Thermo Electron / Tecomet of Woburn, Massachusetts, using the tungsten stack lamination technique described above. The collimator is 7 mm thick, with a bore size of 260 μm , placed in a 64 \times 64 array on a 380 μm pitch. The cell array was centered with 5 mm tungsten on each side, providing an aspect ratio of 27:1. The collimator was placed on top of the aluminum housing of the detector array. Eight screws, two on each side, allowed careful alignment of the collimator with the detector array with the help of a line source. The detector-collimator spacing was 2.3 mm.

III. RESULTS

A. Energy Resolution

In our current data acquisition, the energy of the gamma ray is estimated by summing multiple pixel signals together [8]. When a gamma ray interacts in the crystal, signals can spread to multiple pixels through charge diffusion and the emission of K x-rays from the interaction site. Positive signals are generally confined to two pixels and rarely spread beyond a 3 \times 3 pixel area. To speed data processing, we only analyzed a 3 \times 3 area for each gamma-ray interaction. Whenever we add pixel signals to the sum, there is a tradeoff between the benefit of collecting more of the true signal and the penalty of added noise. We used an experimentally obtained threshold in the sum to minimize the noise while collecting the maximum signal. Any pixel in a 3 \times 3 area that had a signal greater than 3 keV was included in the sum. Figure 3 shows a $^{99\text{m}}\text{Tc}$ spectrum obtained when neighboring pixels in a 3 \times 3 region were summed together. This spectrum has energy resolution of 15 keV full-width-at-half-maximum (FWHM).

We can get better energy resolution than with pixel signal summing when we do maximum-likelihood estimation based on a physical model of the detector [13]. We use simplified models of detector behavior to simulate sets of pixel signals.

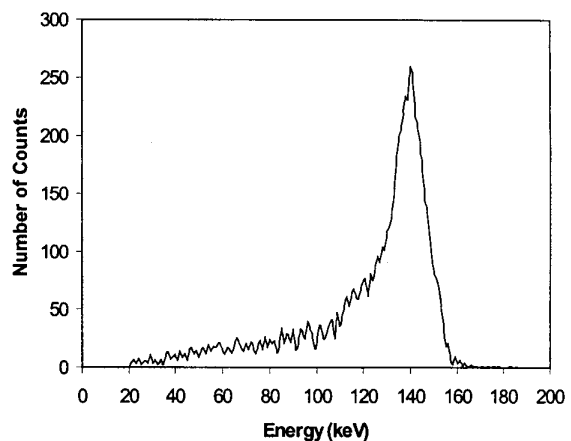


Figure 3: Energy spectrum obtained from averaging a 3 \times 3 pixel area, resulting in 15 keV FWHM energy resolution.

We simulate the effects of two charge deposits: the deposit at the initial interaction site and the deposit generated by an x-ray emitted from the interaction site. A look-up table gives the expected pixel signals as a function of the charge deposit position. In our simplest algorithm, we vary the positions of the charge deposits and the energy of the gamma ray until we find a set of simulated pixel signals that is in least-squares agreement with the observed signals. The energy and interaction position that generate this set of pixel signals are our maximum-likelihood estimates. Figure 4 shows the same set of data when maximum-likelihood estimation is used. This spectrum has 10 keV FWHM, an improvement of over 30% in energy resolution.

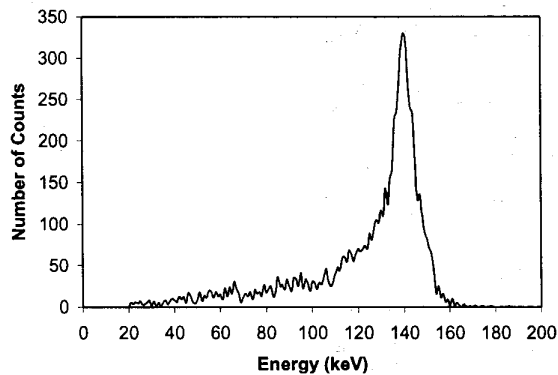


Figure 4: Energy spectrum obtained using maximum-likelihood energy estimation, resulting in 10 keV FWHM energy resolution.

B. Point Response Function

Our system is a continuous-to-discrete imaging system. Consequently, the point response function (PRF) of the system is a function of two variables, the source position and the detector pixel location. Figure 5 shows the (PRF) of the system as a function of the detector pixel location when the source position is fixed. The image was obtained by centering a 300 μCi $^{99\text{m}}\text{Tc}$ (140 keV) point source on one pixel and acquiring an image for 3 minutes. The source was placed 4 mm away from the collimator face, which is the minimum distance for an object in the current set-up. The point source was created using an ion-exchange-resin bead. The bead was placed in a $^{99\text{m}}\text{Tc}$ aqueous solution and then dried to produce a 300- μm circular point source. By fitting a Gaussian curve to a cross-sectional profile of the PRF, we obtained a 450- μm FWHM spatial resolution. The full-width-tenth-maximum (FWTM) was found to be about 1mm. The FWTM is more sensitive to the septal penetration than the FWHM. Since the FWTM is only about 2 times greater than the FWHM, septal penetration is minimal [14].

We also determined septal penetration by obtaining the PRF as a function of the source position. In this case, the PRF was obtained by moving the same point source along the detector plane and registering the number of counts recorded

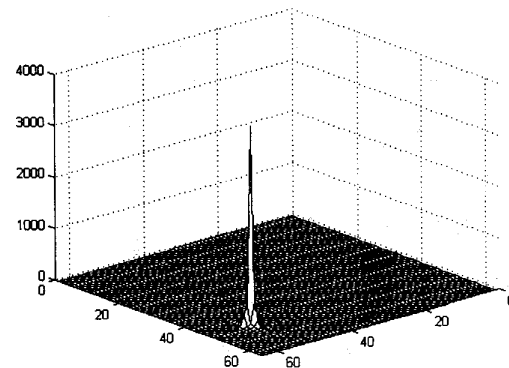


Figure 5: Point response function of the system for fixed source position at 140 keV, resulting in 450- μm FWHM spatial resolution.

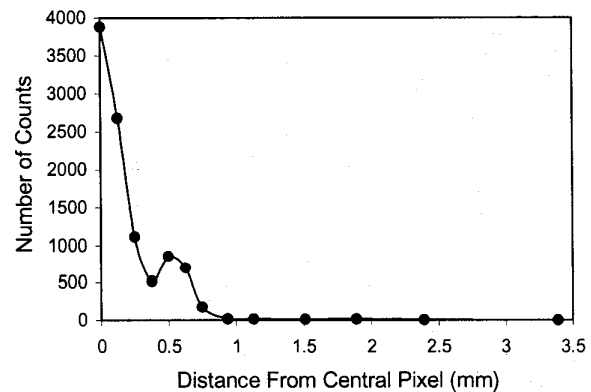


Figure 6: Point response function of the system as a function of the source position for a fixed pixel location.

at a particular central pixel. We moved the source as far as 3.5 mm away from the central pixel location until the number of counts recorded remained constant. Figure 6 shows the number of counts at the central pixel as a function of the distance of the source away from it. The plot indicates that there is little penetration when the source is more than about 1 mm away from the central pixel location. This result is in agreement with the FWTM obtained from the point response function shown in Figure 5.

IV. IMAGES

We assessed the resolution properties of the system by imaging both phantoms and live animals. For phantom imaging we used a line phantom consisting of a capillary tube filled with $^{99\text{m}}\text{Tc}$ aqueous solution. Two such tubes were filled with 1 mCi $^{99\text{m}}\text{Tc}$ and placed in contact with each other 4mm away from the collimator. The capillaries had a 500 μm inside diameter and 1.5 mm outside diameter. We acquired a five-minute image for a total of 100,000 counts. The resulting



Figure 7: Capillary tubes of 500 μm inside diameter in contact with each other, consistent with sub-millimeter resolution.



Figure 8: Femoral node of a rat. A lymphatic channel is visible from the injection site to the node.

image is shown in Figure 7, where the separation of the lines is consistent with sub-millimeter resolution.

We imaged the skeleton of a mouse and the lymphatic system of a rat. We used Nembutal to anaesthetize the rat and a Xylazine/Ketamine solution for the mouse. For lymphatic imaging, we intradermally injected a 500 g rat with 250 μCi $^{99\text{m}}\text{Tc}$ -human serum albumin in the hind limb and imaged immediately after injection. In the image of Figures 8 we can resolve the lymphatic channels extending from the injection site to the femoral node. All animal images were flood-corrected to compensate for local variations in detector sensitivity. Furthermore, we applied an expectation-maximization (EM) reconstruction algorithm based on experimental characterization of the detector response. The images were also smoothed using bilinear interpolation.

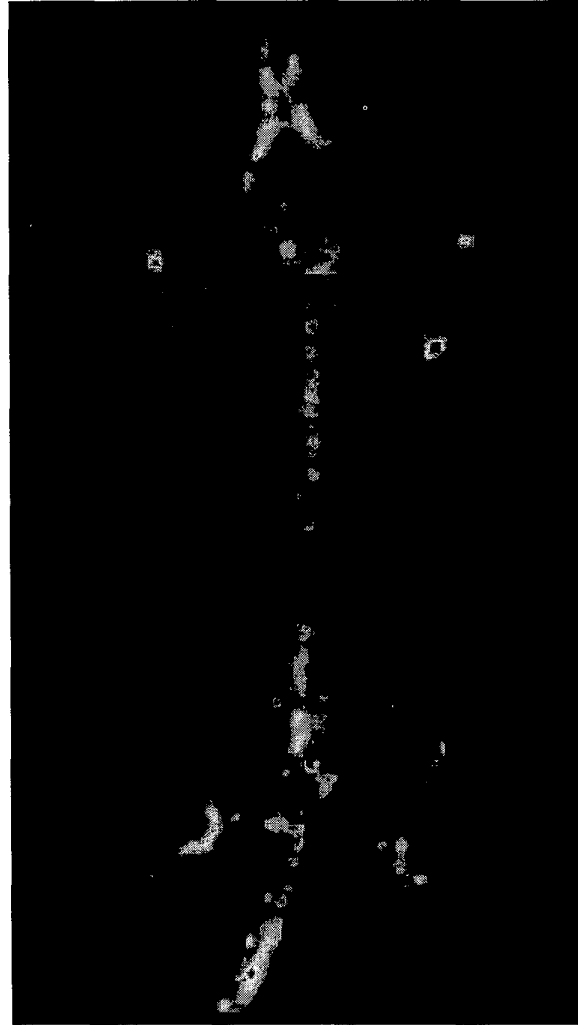


Figure 9: An image of the whole mouse composed of 7 five-minute images obtained by longitudinally shifting the animal.

We acquired skeletal images of a 25 g mouse at three hours after tail-vein injection of 15 mCi $^{99\text{m}}\text{Tc}$ -methylene diphosphonate. We positioned the animal in the prone position 4 mm away from the collimator and obtained 7 five-minute images by longitudinally shifting the mouse. The final image shown in Figure 9 is a mosaic of the acquired images. Each image has between 30,000 and 50,000 counts. The image in Figure 10 is a simultaneous image of the "hot" tail with the right hind limb. This image indicates, once again, that septal penetration due to a strong source close to the collimator face is not significant. Individual digits of the hind limb can be identified when the image is displayed in a logarithmic scale. The images clearly demonstrate anatomical features of the individual vertebrae of the spine as well as the individual digits in the hind limbs.

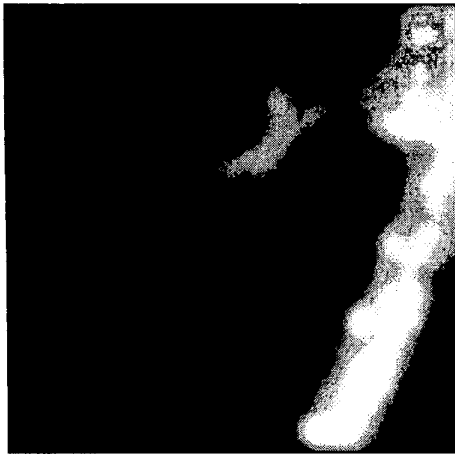


Figure 10: A simultaneous image of the "hot" tail with the hind limb where individual digits can be resolved. The image is displayed in a logarithmic scale so that both the limb and the tail can be seen.

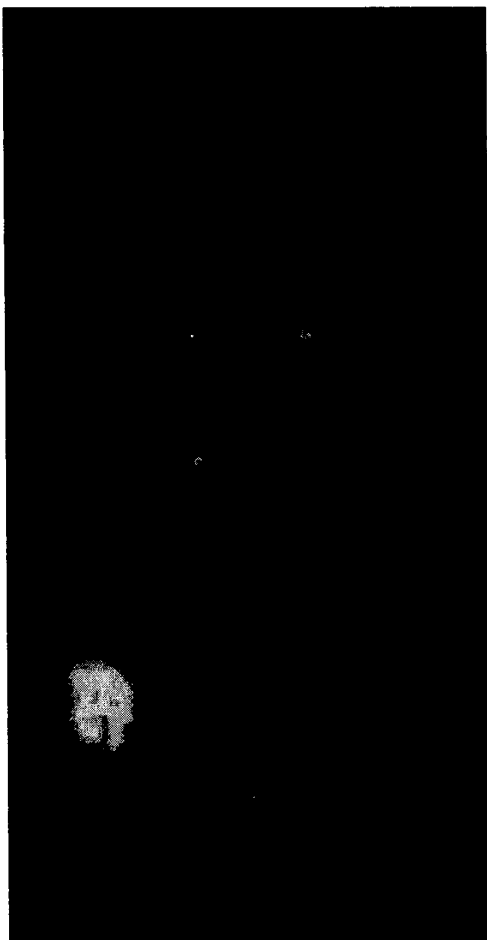


Figure 11: Image of the vertebral column with the mouse in supine position. Individual vertebrae can be resolved in detail.

We also collected images of the mouse in the supine position. In this position the spine is closer to the collimator, resulting in a higher-resolution image. Figure 11 is a combination of two 30-minute images. Details of the vertebrae, which are approximately 3-5 mm in diameter, can be resolved. Other visible structures include pelvis, kidneys and bladder.

V. CONCLUSIONS

We have tested a CdZnTe semiconductor array with a high-resolution collimator for applications in nuclear medicine. The detector-collimator system produced sub-millimeter-resolution animal images in a one-inch-square field-of-view. The acquired images indicate that high-resolution semiconductor arrays can play an important role in the development of small-animal imaging systems. Nuclear medicine imaging provides an attractive method for serial assessment of small animals since it allows each animal to act as its own control, thereby providing information on the progress of disease. The hybrid detector array and collimator described here can be used for planar imaging or implemented in a semiconductor SPECT imaging system.

VI. ACKNOWLEDGMENTS

The author would like to thank George McNeill and the technical staff of the Division of Nuclear Medicine of University Medical Center at the University of Arizona for support with the radiotracers. We would like to further thank Dr. A. Cress and L. Lee for providing the animals, G.D. Paine-Murrieta and K. Salam for helping with the animals, J. Sain for helping with the system, and Dr. A. Brill for suggesting the procedure for making very small point sources. The work was supported by National Institutes of Health Grant RO1 CA75288 and P41 RR14304. George Kastis is a scholar of the "Alexander S. Onassis" Public Benefit Foundation under Group-T040.

VII. REFERENCES

- [1] S.R. Cherry, Y. Shao, R.W. Silverman, K. Meadors, S. Siegel, A. Chatziioannou, J.W. Young, W. Jones, J.C. Moyers, D. Newport, A. Boutefnouchet, T.H. Farquhar, M. Andreaco, M.J. Paulus, D.M. Binkley, R. Nutt, M.E. Phelps, "MicroPET: a high resolution PET scanner for imaging small animals," *IEEE Trans. Nucl. Sci.*, vol. 44, no. 3, 1161-1166, 1997.
- [2] G.K. Kastis, H.B. Barber, H.H. Barrett, H.C. Gifford, I.W. Pang, D.D. Patton, J.D. Sain, G. Stevenson, D.W. Wilson, "High resolution SPECT imager for three-dimensional imaging of small animals," *J. Nucl. Med.*, vol.39, no. 5(suppl.), 9P, 1998.
- [3] Y. Eisen, A. Shor, C. Gilath, M. Tsabarim, P. Chouraqui, C. Hellman, E. Lubin, "A gamma camera based on CdTe

- detectors," *Nucl. Instr. and Meth. in Phys. Res. A*, vol. 380, no. 1-2, 474-478, 1996.
- [4] J.F. Butler, C.L. Lingren, S.J. Friesenhahn, F.P. Doty, W.L. Ashburn, R.L. Conwell, F.L. Augustine, B. Apotovsky, B. Pi, T. Collins, S. Zhao, C. Isaacson, "CdZnTe solid-state gamma camera," *Conference Record of the 1997 IEEE Nucl. Sci. Symp.*, IEEE, New York, NY, vol. 1, 281-285, 1997.
- [5] C. Scheiber, B. Eclancher, J. Chambron, V. Prat, A. Kazandjan, A. Jahnke, R. Matz, S. Thomas, S. Warren, M. Hage-Hali, R. Regal, P. Siffert, M. Karman, "Heart imaging by cadmium telluride gamma camera European Program "BIOMED" consortium," *Nucl. Instr. and Meth. in Phys. Res. A*, vol. 428, no. 1, 138-149, 1999.
- [6] H.B. Barber, H.H. Barrett, E.L. Dereniak, N.E. Hartsough, D.L. Perry, P.C.T. Roberts, M.M. Rogulski, J.M. Woolfenden, E.T. Young, "A gamma-ray imager with multiplexer readout for use in ultra-high-resolution brain SPECT," *IEEE Trans. Nucl. Sci.*, vol. 40, no. 4, 1140-1144, 1993.
- [7] H.B. Barber, D.G. Marks, B.A. Apotovsky, F.L. Augustine, H.H. Barrett, J.F. Butler, E.L. Dereniak, F.P. Doty, J.D. Eskin, W.J. Hamilton, K.J. Matherson, J.E. Venzon, J.M. Woolfenden, E.T. Young, "Progress in developing focal-plane-multiplexer readout for large CdZnTe arrays for nuclear medicine applications," *Nucl. Instr. and Meth. in Phys. Res. A*, vol. 380, no. 1-2, 262-265, 1996.
- [8] D.G. Marks, H.B. Barber, H.H. Barrett, E.L. Dereniak, J.D. Eskin, K.J. Matherson, J.M. Woolfenden, E.T. Young, F.L. Augustine, W.J. Hamilton, J.E. Venzon, B.A. Apotovsky, F.P. Doty, "A 48x48 CdZnTe array with multiplexer readout," *IEEE Trans. Nucl. Sci.*, vol. 43, no. 3, 1253-1259, 1996.
- [9] K.J. Matherson, H.B. Barber, H.H. Barrett, J.D. Eskin, E.L. Dereniak, D.G. Marks, J.M. Woolfenden, E.T. Young, F.L. Augustine, "Progress in the development of large-area modular 64x64 CdZnTe imaging arrays for nuclear medicine," *Conference Record of the 1997 IEEE Nucl. Sci. Symp.*, IEEE, New York, NY, vol. 1, 276-280, 1997.
- [10] H.B. Barber, H.H. Barrett, F.L. Augustine, W.J. Hamilton, B.A. Apotovsky, E.L. Dereniak, F.P. Doty, J.D. Eskin, J.P. Garcia, D.G. Marks, K.J. Matherson, J.M. Woolfenden, E.T. Young, "Development of a 64x64 CdZnTe array and associated readout integrated circuit for use in nuclear medicine," *Journal of Electronic Materials*, vol. 26, no. 6, 765-772, 1997.
- [11] J.M. Woolfenden, H.B. Barber, H.H. Barrett, E.L. Dereniak, J.D. Eskin, D.G. Marks, K.J. Matherson, E.T. Young, F.L. Augustine, "Modular 64x64 CdZnTe arrays with multiplexer readout for high-resolution nuclear medicine imaging," *Semiconductors for Room-Temperature Radiation Detector Applications II*, R.B. James et al., eds., *Mat. Res. Soc. Symp. Proc.*, vol. 487, 239-243, 1998.
- [12] A. Valda Ochoa, L. Ploux, R. Mastroppolito, Y. Charon, P. Laniece, L. Pinot, L. Valentin, "An original emission tomograph for *in vivo* brain imaging of small animals," *IEEE Trans. Nucl. Sci.*, vol. 44, no. 4, 1533-1537, 1997.
- [13] D.G. Marks, H.B. Barber, H.H. Barrett, J.D. Eskin, "Maximum-likelihood estimation for semiconductor detector arrays," *Conference Record of the 1997 IEEE Nucl. Sci. Symp.*, IEEE, New York, NY, vol. 1, 551-555, 1997.
- [14] D.C. Gunter, "Collimator characteristics and design," *Nuclear Medicine*, R.E. Henkin et al., eds., Mosby, New York, NY, vol. 1, 96-124, 1996.